A phantom-based evaluation of a real-time tracking micro MLC delivery

Yaxi Liu*

Radiation Oncology Department

Cancer Therapy & Research Center, San Antonio, TX, USA

University of Texas Health Science Center at San Antonio, TX, USA

Tel: +1 210 450 1658, Fax: -1 210 616 5682

*Corresponding author, E-mail: yliu@ctrc.net

Fan-chi Su

Radiation Oncology Department

Cancer Therapy & Research Center, San Antonio, TX, USA

University of Texas Health Science Center at San Antonio, TX, USA

Martin Szegedi

Radiation Oncology Department

University of Texas Health Science Center at San Antonio, TX, USA

Lan Lin

Lan Lin, Ph.D.

Radiation oncology department

Mary Bird Perkins Cancer Center, Baton Rouge, LA, USA

Chengyu Shi

Radiation Oncology Department

Cancer Therapy & Research Center, San Antonio, TX, USA

University of Texas Health Science Center at San Antonio, TX, USA

Niko Papanikolaou

Radiation Oncology Department

Cancer Therapy & Research Center, San Antonio, TX, USA

University of Texas Health Science Center at San Antonio, TX, USA

Biographical notes: Y Liu received his PhD in nuclear engineering from North Carolina State University in 2006. He is currently Assistant Professor at the Department of Radiation Oncology, University of Texas Health Science Center at San Antonio, TX. His current research interests include dose algorithm optimization, Monte Carlo simulation, 4D real-time tracking RT, and medical device R&D for IMRT and SRT.

F. Su is a PhD candidate in the Department of radiation oncology, UTHSCSA.

M. Szegedi is a PhD candidate in the Department of radiation oncology, UTHSCSA.

L. Lin received her PhD in the Department of radiation oncology from UTHSCSA in 2007.She is currently a medical physicist at Mary Bird Perkins Cancer Center. Her research interests focus on 4D treatment planning, 4D treatment delivery and image guided radiation therapy.

C Shi received his PhD in nuclear engineering from Rensselaer Polytechnic Institute in 2004. He is currently Assistant Professor at the Department of Radiation Oncology, UTHSCSA and medical physicist in Cancer Therapy & Research Center. His research interests cover various aspects in radiation detection, radiation dosimetry, the Monte Carlo method, medical image segmentation, registration, and 4D simulation.

N Papanikolaou received his PhD in medical physics from University of Wisconsin-Madison, School of Medicine. He is currently Professor at the Department of Radiation Oncology, UTHSCSA and the Director of Medical Physics Department in Cancer Therapy & Research Center. His current interests include dose computation, optimization, and image guided radiotherapy.

Abstract: A Real-time Tracking Radiation Therapy (RTRT) system was developed as a retrofit to an existing linear accelerator. The system includes a dual-layer micro MLC collimator (mMLC) and an integrated portal imaging camera system. The RTRT system allows the user to follow the tumor position during the treatment and compensate for the intra-fractional tumor motion by adjusting the position of each mMLC leaf. We have performed evaluations of the tracking position accuracy, mMLC motion time delay, dosimetric accuracy, and tracking failure rate. The dose difference of radiographic films between the No-tracking pattern and the Static pattern was 55.58% over the selected tolerance of 10%. The dose difference between the No-tracking pattern and the Tracking pattern was 49.14% over the tolerance. With tracking, the dose difference between the Tracking pattern and the Static pattern was 11.64% over the tolerance. Our results indicate that real-time tracking system provides considerable advantages with more accurate delivery of dose to the moving target as compared to current non-tracking and gating techniques.

Keywords: dual-layer micro MLC, intra-fractional motion, real-time tracking, radiation therapy

1 Introduction

Advances in three-dimensional (3D) treatment technique, such as 3D radiotherapy (RT) and intensity modulation radiotherapy (IMRT) and the implementation of image-guided radiotherapy (IGRT) techniques have reduced inter-fractional tissue shifts in the course of radiation therapy. The improvements lead to the potential of reductions in PTV margins and consequently improvements in normal tissue complications as well as potential escalation in target dose.

While we have overcome rigid organ motion among treatment fractions, today's RT treatment still faces the difficulty to account for intra-fractional tissue motion. Changes in the breathing frequency and organ motion are in general irregular, displaying location and shape variation of the anatomy over the course of the treatment as well as during each treatment fraction. These are vital variables that should be accounted for when using motion controlling techniques. Murphy et al (2004) showed that a slow, steady drift of tumor position occurs in the breath-holding technique during an extended sequence of held breaths. Complex tumor motions in lung and abdominal region, resulting from motions in the soft tissue due to breathing show mostly hysteretic motion patterns. (Murphy MJ, 2004, Keall P et al. 2005) and account for one of the largest displacements observed (Lujan et al. 1999).

Intra-fractional tumor motion causes movement in the centimeter range (Shirato H. et al. 2004, Brandner ED, et al. 2006) and counteracts the potential of highly conformal dose delivery in 3D or IMRT modalities. The treatment outcome, thus, is an undesirable dose to normal healthy tissue and underdose in tumor periphery and edge.

Various ways have been developed to accommodate for tumor motion (Hugo GD et al. 2006). Most notably a temporarily controlled beam-delivery to time points at which the tumor is in the previously planned position, such as in gated RT (Mageras GS, 2004, Dietrich L et. al. 2005, George R et. al. 2006, Kubo and Wang 2000, Zhang T 2004).

Possible solutions for gating radiotherapy range from voluntarily patient-controlled breath hold to semi-forced breath hold devices, which guide a patient and allow for treatment interruption and the controlled beam interrupt during cyclic phases. The common aim is to generate a quasi 3D-static situation, allowing planning of a treatment with reduced margins around the target.

Most of the proposed delivery strategies requires a patient specific evaluation to counter potential disadvantages (Vedam SS 2001) such as the generally extended treatment time as the tumor moves outside the declared margin (resulting in beam-off time) and a lowered duty-cycle of a linear accelerator. Extended treatment times have been shown to decrease patient comfort and increase the possibility of patient motion. Breath-holding techniques are unsuitable for compromised lung performance as it is often the case with lung cancer patients (Mageras and Yorke, 2004).

The other solution to motion suggested is using the beam to follow the tumor motion, i.e. Real-time tumor tracking. Several studies have been conducted over the past years. The most advanced of which is the Cyberknife system as introduced by Schweikard et al 2004. Here the whole gantry is moved to follow tumor motion. Keall et al. (2005) have extracted motion from 4D CT scans and applied these to modify dynamic multileaf collimator (MLC) movements, showing the feasibility of MLC adapted tracking. A couch based approach by D'Souza (2005) shows similar feasibility, allowing a clearer distinction of beam shaping- and motion-compensating movements.

While correction in all three motion dimensions would be ideal, Nill et al (2005) have evaluated the effect of directional imaging to detect and minimize intra-fraction motion. They concluded that the correction in beam direction seems more important by assuming corrections for breathing only as inter-fractional shifts have been taken care during setup. Our approach fosters their results and the beam alignment is maintained only in the plane of the treatment field. Uncompensated out-of-plane translation represents only a small effect compared with in-plane translations, but if the tumor rotates out-of-plane the dose conformality can be compromised.

To accomplish motion compensation in real time and to accommodate for the intra-fractional changes, one needs a predictive algorithm foreseeing the position of a planned target value (PTV).

We have evaluated the feasibility to use a stereotactic micro MLC (mMLC) system to track tumors. A technical description has been published by (Bucciolini et al. 2002, Liu Y[1,2], et al 2007). Knowledge of the target position at all times is a pre-requisite of our technique and has been achieved by implanted radiopaque fiducial markers inside or near the target. Due to the unique possibility to adjust leafs in two dimensions, motion compensation fully affects the 2D plane perpendicular to the beam direction.

This manuscript presents first phantom measurement results to study the effects of target motion on dose distributions systematically for a stereotactic delivery system. Differences between dose distributions for static targets and those achieved with motion compensation for moving targets are compared to evaluate the feasibility of 3D/IMRT beam tracking for motion compensation and also to evaluate the capabilities of the treatment machine to deliver such treatments.

2 Method and Materials

The Real-time Tracking Radiation Therapy (RTRT) system is an integrated system which includes its kernel image processing tools (IPT), the dual-layer micro MLC, and the communications between IPC and mMLC. The following sections describe the system architecture, the image processing tools and the key devices which we used for the RTRT experiments.

2.1 Real-time Tracking Radiation Therapy architecture

The following block diagram below illustrates the **r**eal-time **t**racking **r**adio**t**herapy (RTRT) architecture. The architecture consist two major parts, the devices and the IPT. The devices include a megavoltage (MV) X-ray beam, a moving target with marker, a MV image detector, and MLC. The basic idea of this RTRT architecture is to move MLC leaves to form a tracking beam according to the motion of target. The main diagram consists of four steps, as shown in Figure 1.

Step A collects the MV fluence by the image detector. The fluence is obtained through a moving target with an implanted marker inside. The marker creates a contrast area which is identified as the marker position is projected to the image detector.

Step B transfers the collected MV fluence image to the image processing tools.

Step C provides the connection between the IPT and MLC leaf controller. After the MV image is processed, a MLC leaf controller file is generated and delivered to MLC Leaf Controller.

Step D provides the tracking beam which is generated by re-positioning MLC leaves according to the target motion.

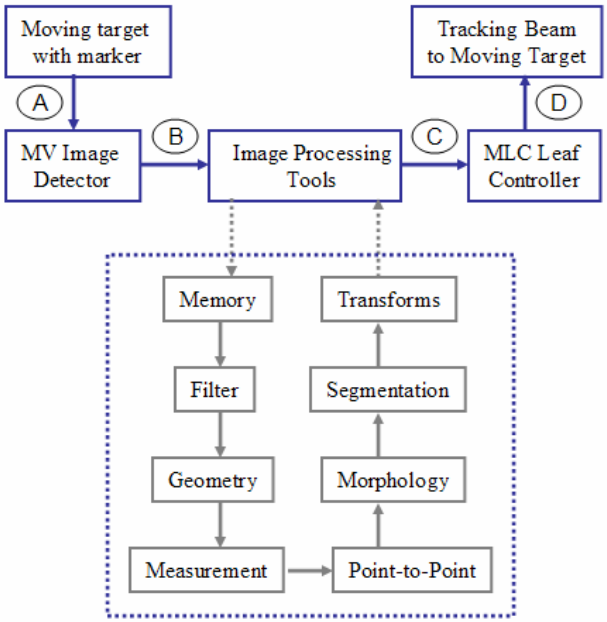

Figure 1: Block diagram of Real-time Tracking Radiation Therapy architecture

Image Processing Algorithm

The Image Processing Tools (IPT) play the most important role in the integrated system. The IPTs' set of specific modules, as shown in Figure 1, is described below. The function of the IPT is to convert the MV image which indicates the moving marker position to the MLC leaf controller. IPT is a set of C++ classes and ActiveX controls including low and high-level image processing and analysis functions. These modules include Filter module, Memory module, Geometry module, Measurement module, Morphology module, Point-to-Point module, Segmentation module, and Transforms module

The Memory module provides support for allocating and manipulating images and vectors. It includes specific functionality for managing the processing kernel and lookup table.

The Filter module provides support for a set of commonly used linear shift-invariant filters to perform edge detection, smoothing, line detection, and image enhancement. Generalized convolutions are available for both one and two-dimensional processing.

The Geometry module provides support for performing geometric transformations such as shearing, rotating, flipping, warping, and resizing of images.

The Measurement module provides support for measuring and/or visualizing some characteristics of an image. These include operators that produce histograms, projections, correlations, and pixel value statistics for an image or regions-of-images.

The Morphology module provides support for morphological opening, closing, dilation, and erosion on both binary and gray scale images. Other functions included in this module are operators that perform rank value filtering, skeletonizing, hit or miss, thickening, thinning, and outlining.

The Point-to-Point module provides support for manipulating images on a pixel by pixel basis. These functions were used for performing binary and unary arithmetical operations, gray-scale mapping, threshold, and equalization.

The Segmentation module provides support for extracting and manipulating higher level representations of images by grouping image pixels into regions of uniform brightness.

The Transform module provides support for transforming an image from one domain to another.

Adaptive Function in TrackBeam

Since the time delay, experienced between the mMLC positioning and the moving markers, is one of the major factors that can cause errors in any target tracking system we have implemented the adaptive function, which reduces the positioning lag. In the TrackBeam, the adaptive function was developed based on the Kalman filter (KF). A KF (Kalman, 1960, Kalman and Bucy 1961) is based on linear dynamical systems discretised in the time domain. These play a fundamental role in handling structural time series models, which are formulated directly in terms of components of interest (Harvey, 1989) and have been originally developed and exploited in control engineering.

The KF is a predictor-corrector type estimator by implementing a set of mathematical equations and functions. It minimizes the estimated error covariance—if some presumed conditions are met. The Kalman filter is a recursive estimator, which means that the estimated state from the previous time step and the current measurement are needed to compute the estimate for the current state.

If the state transition and observation models are highly non-linear, the extended Kalman filter can give particularly poor performance [Julier, 1997]. This is because only the mean is propagated through the non-linearity. The unscented Kalman filter (UKF) [Julier, 1997] uses a deterministic sampling technique known as the unscented transform to pick a minimal set of sample points (called sigma points) around the mean. These sigma points are then propagated through the non-linear functions and the covariance of the estimate is then recovered.

The Kalman filter has been increasingly used in a wide variety of areas such as for motion prediction (Azuma and Bishop 1994; Azuma 1995), and for multi-sensor (inertial-acoustic) fusion wide area tracking system (Foxlin, Harrington et al. 1998, Welch, Bishop et al. 2001).

2.2 MV Tracking Devices

Dual-layer Micro Multileaf collimator (DmMLC)

A dual-layer micro multileaf collimator (DmMLC) by Initia Medical Technology (Canton, MA), was mounted on the Varian 600C. This dual-layer mMLC has 96 tungsten leaves divided into four banks, each consisting of 14 inner leaves and 10 outer leaves with leaf width at isocenter as 3.5 mm and 5.0 mm, respectively. The DmMLC consists of the upper (Y-axis travel) and the lower (X-axis travel), dual layers, of leaves, as shown in Figure 2. The upper and lower layers of MLC leaves are perpendicular to the central axis and travel orthogonally to each other providing a maximum field size of 10 cm x 10 cm with a leaf width of 3.5 mm at isocenter. It was mounted on and commissioned with a Varian 600C linear accelerator machine with photon beam energy of 6 MV. Each leaf is controlled by individual motors, traveling at maximum speeds of 20 mm/sec. The innovative dual layers design offers DmMLC unique features in reducing the dose undulation, the leaf-end transmission and the MLC field dependence of the leaf stepping angle (Liu Y[3], et al 2008). DmMLC travels in two orthogonal directions compared with one direction motion of conventional standard MLC. It also provides the feasibility for precise shaping of complex irregular apertures.

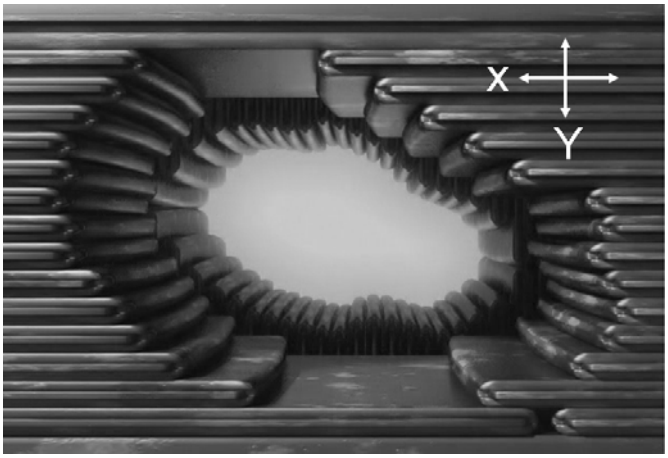

Figure 2: AccuKnife dual-layer mMLC mounted on a Varian Clinic 600C and the axial view of dual layers leaves

Quasar Respiratory Phantom

The QUASAR™ Respiratory Motion Phantom (Modus Medical Devices, Inc. London, ON Canada) is a thorax phantom that is capable of moving in the superior-inferior direction with variable speed and amplitude. Major components of this respiratory phantom system, which is shown in Figure 3a), include a thorax phantom, a precise motion actuator, and a controller with pre-set motion profile. The thorax phantom is composed of a moving insert, which can be switched between a lung equivalent cedar and an optimal Acrylic insert, linked to a moving platform.

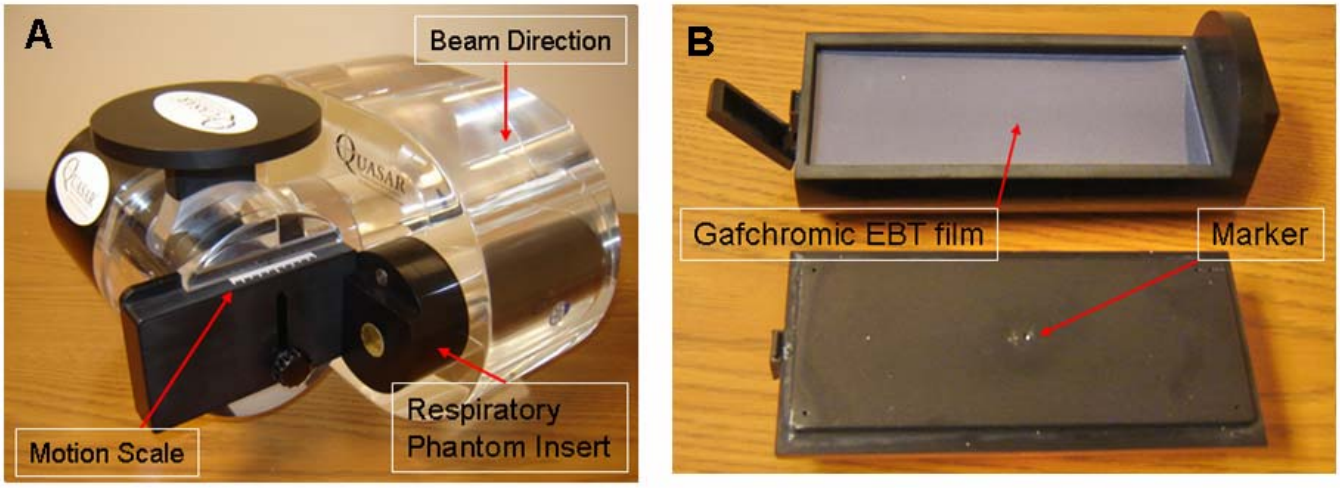

Figure 3: (A) QUASAR Respiratory Motion Phantom, (B) QUASAR respiratory motion phantom insert with Gafchromic EBT film and Marker

The motion of tumors in the moving phantom is achieved by the actuator applying sinusoidal motion to a moving rod. Motion amplitudes of the QUASAR respiratory phantom are up to 40 mm in superior/inferior direction and up to 4 seconds per cycle.

Gafchromic® EBT film

The newly developed Gafchromic® EBT film is a commercially available radiochromic film designed for the measurement of absorbed dose of high-energy photon beams and is particularly attractive for IMRT dosimetry. Gafchromic® EBT films are laminated with two film coatings resulting in an active layer of approximately 17 μm thick. The nominal thickness of 234 μm (ISP, 2006) is ideal for patient dosimetry with minimal perturbation of the delivered dose. As reported by the manufacturer (ISP, 2006), Gafchromic® EBT film is composed of H(39.7%), C(42.3%), O(16.2%), N(1.1%), Li(0.3%), and Cl(0.3%). The maximum light absorption band is centered at 633 nm, and the Z_{eff} is 6.98 (ISP, 2006), which is very close to Z_{eff} of water (7.30). Irradiation of Gafchromic® EBT films with ionization radiation induces a polymerization effect which changes the originally colorless film to shades of blue. Therefore, the measured dose can be estimated directly by analyzing the absorbed spectrum (Gamble et al., 2003). The Gafchromic® EBT films were put in the QUASAR respiratory cassette insert during the following experiments, as shown in Figure 3b).

Dosimetric characteristics of Gafchromic® EBT films for high-energy photon and electron beams have been reported in the literature. Energy independent and field size independent when exposed to either high energy photon or electron beams are main advantages of the Gafchromic® EBT film (Devic et al., 2004 and 2005, Butson et al., 2006; Cheung et al., 2006; Todorovic et al., 2006; Su et al., 2007). Also, the Gafchromic® EBT film is self-developing, hence eliminating the need for processing. The almost water equivalent density, the extended dose range (up to 8Gy), and the consistent and uniform response (better than 1.5%) (ISP, 2006) are some additional characteristics of the EBT films that can be beneficial to IMRT dosimetry and thus real-time tumor tracking.

2.3 Real-time Tracking Experiments Patterns

2.3.1 RTRT system Installation and Experiment Setup

The Figure 4 shows the experiment setup of the real-time tracking for a respiratory moving target. The Quasar respiratory phantom is moving one-dimensional, loaded with Gafchromic films in the film insert. The whole tracking system was mounted to a Varian 600C The X-ray beam goes through the DmMLC and the respiratory phantom. The MV Image Detector collects the MV fluence. The Gaphchronic films collects the irradiation dose during RTRT.

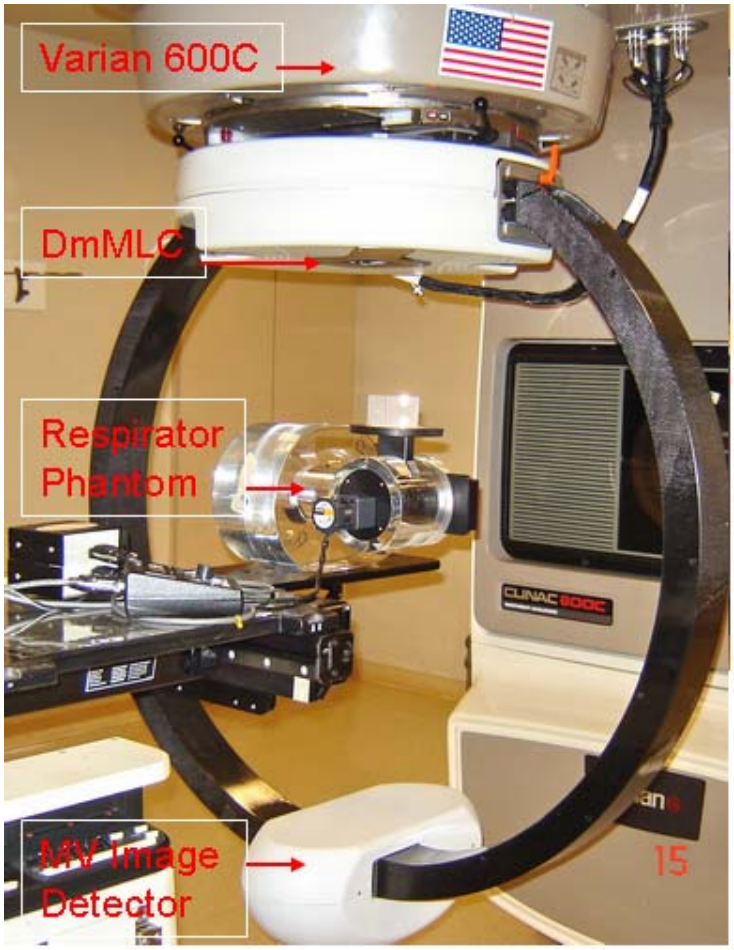

Figure 4: Experimental setup of real-time tracking for respiratory moving target

A workstation was connected with two computers in the control room. One computer was specifically used to display the on-line image of beam and marker. The other computer was used to control the MLC leaf motion. After the phantom was set up and the beam was turned on, the marker could be identified on the screen of the IPT computer. A four-point cursor which forms a 1 cm x 1 cm frame was used to grab the marker as demonstrated Figure 5. The marker moved as the phantom shifted and its motion would be captured by the camera. With a mouse click a frame grabber image was captured as the reference image. For every movement, the IPT processed the real-time moving image and generated the MLC leaf controller file driving each leaf of the DmMLC and forming a new aperture according to the marker motion.

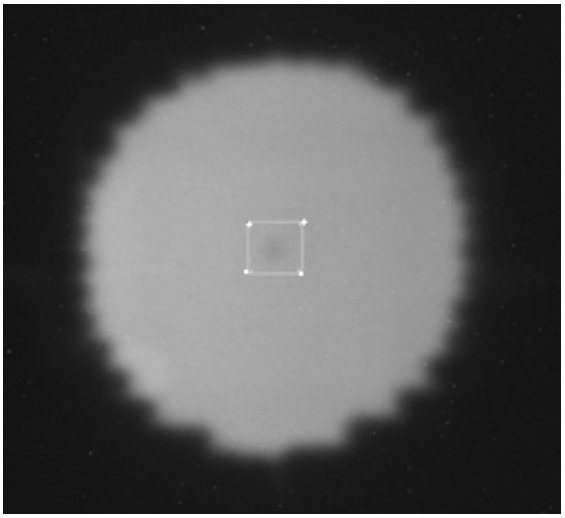

Figure 5: Four points frame grabber at the beginning of tracking

2.3.2 Marker Position Accuracy

In the RTRT system, all tracked leaves were re-positioned during the real-time tracking based on the moving marker. The marker trajectory was processed through the IPT and the trajectory was recorded to evaluate the IPT processing capability. The motion scale in the Quasar respiratory phantom displayed the exact distance for the moving target as it traveled from the end-inhale phase to the end-exhale phase. The trajectory of marker was projected to the Image Detector, processed by IPT and recorded for each individual position. The entire individual trajectory was accumulated in a plot which was capable of showing the marker trajectory during the real-time tracking delivery. A circle of 4 cm in diameter was generated as the aperture shape. During the linac delivery, the dose rate was set up as 320 MU/min and the MU was set to 500 if not specifically mentioned.

2.3.3 Time delay between the marker and the MLC leaf

The time delay between the maker motion and MLC leaf motion was to be evaluated during the tracking. In the beginning, the MLC leaf followed the motion of the marker gradually. Therefore, it is unavoidable to have a time lag between the marker and the MLC. The IPT provided an adaptive function to calculate the time delay between the marker and MLC leaves and offered an adaptive function to minimize the time lag.

2.3.4 Dosimetric analysis for Three Evaluation Patterns with target motion perpendicular to the beam direction

In order to evaluate the effect of real-time tumor tracking, we performed dosimetric comparisons among static, no tumor tracking, and real-time tumor tracking patterns using Gafchromic® EBT films. In our first scenario the tumor is still, thus named Static pattern.

For lung tumors, a realistic assumption during radiotherapy is that the tumor is in motion during the treatment. So the coming two scenarios were set using the motion phantom.

Currently our clinic applies a static leaf pattern (without tracking) towards moving targets, such as in lung cancer. We applied a small margin to allow comparison to the Static pattern and our tracking modus. This was the No-tracking pattern.

The case of a motion target with moving leafs (i.e. with tracking) in the series of our experiment was named Tracking pattern.

A golden seed with 2 mm in diameter which can be imaged by the electronic portal image detector (EPID) of DmMLC system was placed in the phantom to indicate the tumor center. In these three patterns, the dose rate was 320 MU/ min and

the dose to the tumor was 150 cGy. DmMLC was set to generate a circle aperture radiation field with 4 cm in diameter when the beam was perpendicular to the phantom film insert. The tumor motion was simulated in a 5 sec/cycle sigmoid pattern with amplitude of +/- 15 mm in the superior-inferior (SI) direction. There is neither prediction for the tumor motion nor DmMLC synchronization between the DmMLC and tumor center in the no-tracking pattern. On the other hand, tumor motion would be predicted within the first 1 to 4 motion cycles, and then predicted tumor motion would be synchronized with DmMLC delivery in the real-time tumor tracking pattern. Gafchromic® EBT samples (150.0 mm x 65.0 mm in size) were cut from the same batch and placed in the moving insert of the Quasar Respiratory Phantom to evaluate dosimetric accuracy in these three patterns.

2.3.5 Dosimetric analysis of Patterns with target motion in the beam direction

The mMLC-based tracking system uses the projection of the marker to locate the target position. It lacks the capability to track a marker's motion if the target travels in the beam direction. In other words, the tracking system is a two-dimensional tracking system instead of a three-dimensional system. In order to evaluate the dosimetric performance when the target travels in the beam direction, an additional evaluation patterns, named as In-beam-direction Pattern, was investigated. In this experiment setting up, the Gafchromic film was put on the bottom surface of Quasar phantom insert with 5.0 cm solid water as buildup. The gantry rotates 90^0 from that in the Figure 4 and the phantom moves in the central axis of beam. The phantom insert moves -1cm to +1 cm from the SSD = 100 cm setting up. As solid water was attached on the insert bottom surface, the Quasar insert is only capable of moving at a distance of 2 cm instead of 3 cm in the tracking patterns mentioned above. The film attached to the phantom insert moves from 99 cm to 101 cm along the beam central axis. A Gafchromic film with motion in the beam direction was compared with a Gafchromic film of static phantom with film at SSD = 100 cm.

2.3.6 Tracking Failure assessment

As this RTRT system is first-of-its-kind in a pre-clinic stage. Three test scenarios were used to evaluate the tracking failure possibility.

The first test pattern was to assess marker size effect on the tracking capability. The marker was projected to the Image Detector through the treatment beam and its contrast could be detected. By changing the marker size, the contrast between the implanted marker and the target changed. The size of the marker has effect on the contrast which was to be evaluated. A series of gold markers with sizes ranging from 1.0 mm to 5.0 mm in diameter was tested.

The second test pattern for tracking failure was to change the speed of marker motion. A typical patient respiratory cycle takes between 4 to 6 seconds moving the marker from the end-inhale phase to the end-exhale phase in 2 to 3 seconds. The distance of the moving range of the tracking target was set to 30 mm. The target moving speed was set from 10 mm/sec to 15 mm/sec.

The third failure assessment was to evaluate an unexpected tracking failure of this system using the previously determined proper marker size and target moving speed. This test pattern was to repeat the same tracking experiment multiple times to indicate the systematic uncertainty.

3 Results

The section includes results based on the position test patterns, the time delay, the dosimetric results and analysis, and the tracking failure assessment.

3.1 Position accuracy

Figure 6 shows the integrated marker trajectory when the respiratory phantom moves from the end-inhale phase to end-exhale phase at a distance of 30 mm and at a respiratory rate of 5 sec/cycle. The total delivery time in the test was 150 seconds which means 30 cycles of marker trajectory were recorded and displayed in Figure 6. The grid size in this figure is 1 mm.

The integrated mark trajectory is accumulated in a straight line which is the projection of marker motion. The vertical distance from the trajectory bottom to the top is exactly 30 grid which matches well with the marker motion distance as 30mm. The horizontal vibration of the trajectory was within the 1 mm range. The Figure 6 demonstrated the MV Image Detector of the tracking system is capable of accurately detecting the marker trajectory.

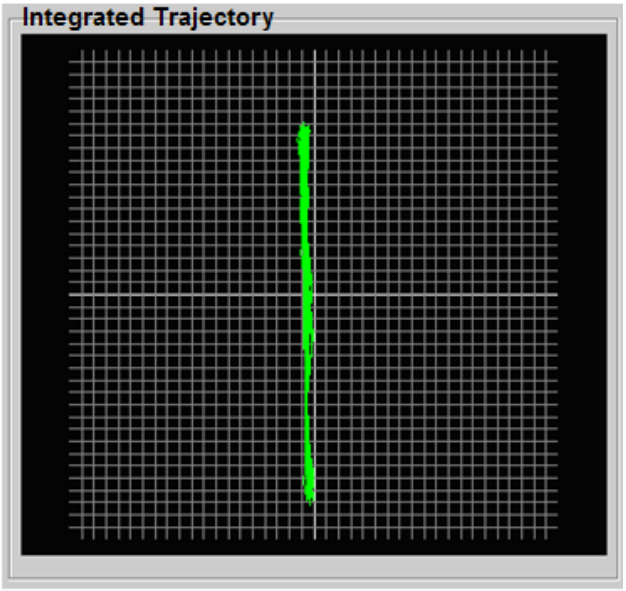

Figure 6: The integrated marker trajectory of RTRT with the grid size as 1 mm

3.2 Time delay between MLC motion and Target motion

The real-time tracking system has a maximum 0.1 to 0.2 seconds time delay between the DmMLC motion and the target motion during the first 1-4 cycles (motion elongation 30 mm, 5 sec/cycle). Since the IPT provided the adaptive function to minimize the time delay, the synchronization of marker motion and the DmMLC leaf motion was achieved within less than 0.05 seconds based on the measurements of trajectory and DmMLC leaf position.

3.3 Dosimetric analysis of radiographic films when target motion perpendicular to beam direction

Figure 7 indicated the result of Gafchromic® EBT films. As we can see, in the No-tumor tracking pattern, the irradiation field was blurred due to tumor motion and resulted in a distortion shape along the moving direction (SI direction). On the other hand, the irradiation field with real-time tumor tracking was rounded with less blur as compared to the No-tracking pattern.

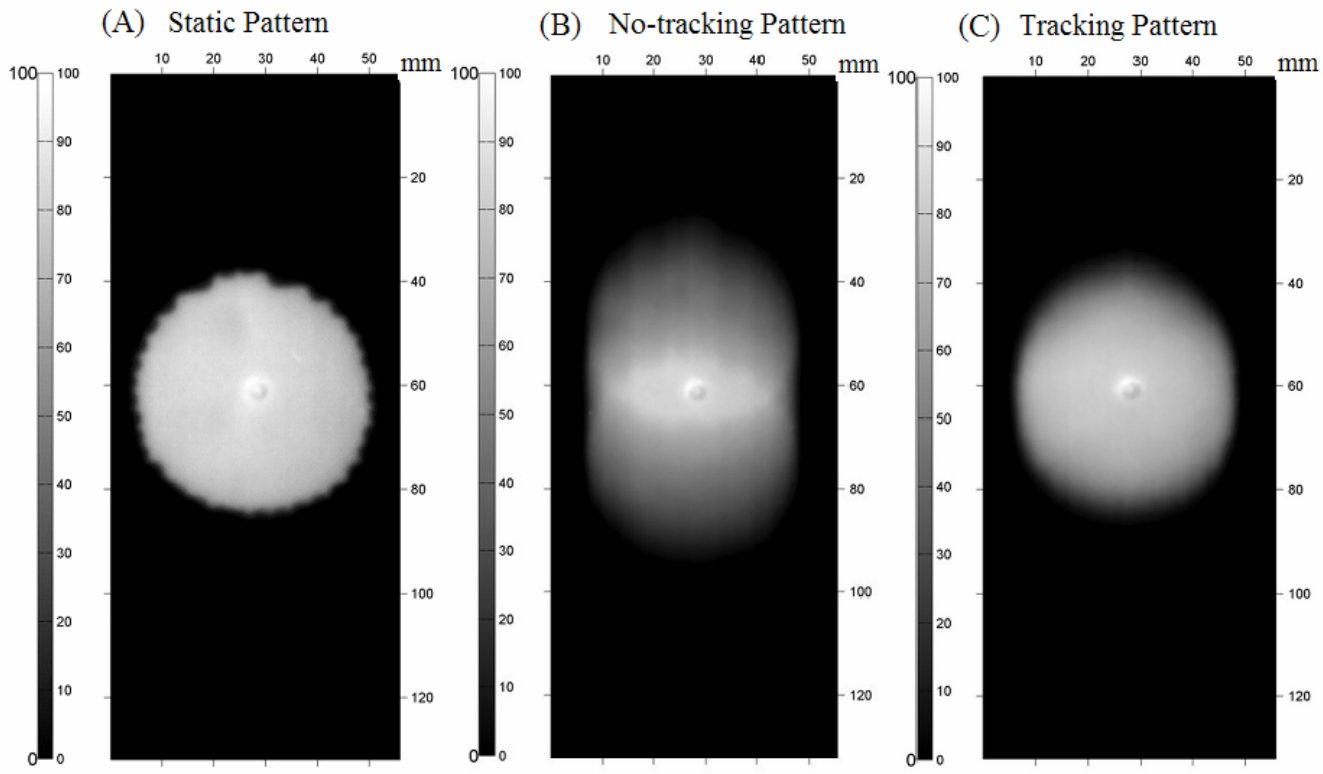

Figure 7 Radiographic films of (A) Static pattern, (B) No-tracking pattern, and (C) Tracking patterns

After the dose conversion from the absorbed spectrum of Gafchromic® EBT films, comparisons of isodose distributions among Static, No-tracking, and real-time Tracking patterns were analyzed below.

3.3.1 No-tracking pattern VS Static pattern

Figure 8 indicated dosimetric comparisons between Static, which is considered as the ideal case in radiation treatments, and No-tracking situations. From the isodose distributions in Figure 8a), we can see that if we did not track tumor motion at all in this small, 4 cm in diameter treatment field situation, the tumor coverage by the 80% isodose line would be much inferior to what we expect in an ideal situation. Also the dose differences over the irradiation field between Static and No-tracking patterns would be significant.

Figure 8b) showed the dose vertical profile along the central axis of the Static pattern and No-tracking patters. The solid line profile was for the Static pattern. It shows an expected dose distribution with a dose plateau along the vertical central axis. The dashed line displays the dose vertical profile for the No-tracking pattern in which the dose accumulates in the middle area and delivers considerable amount of dose to the outside field.

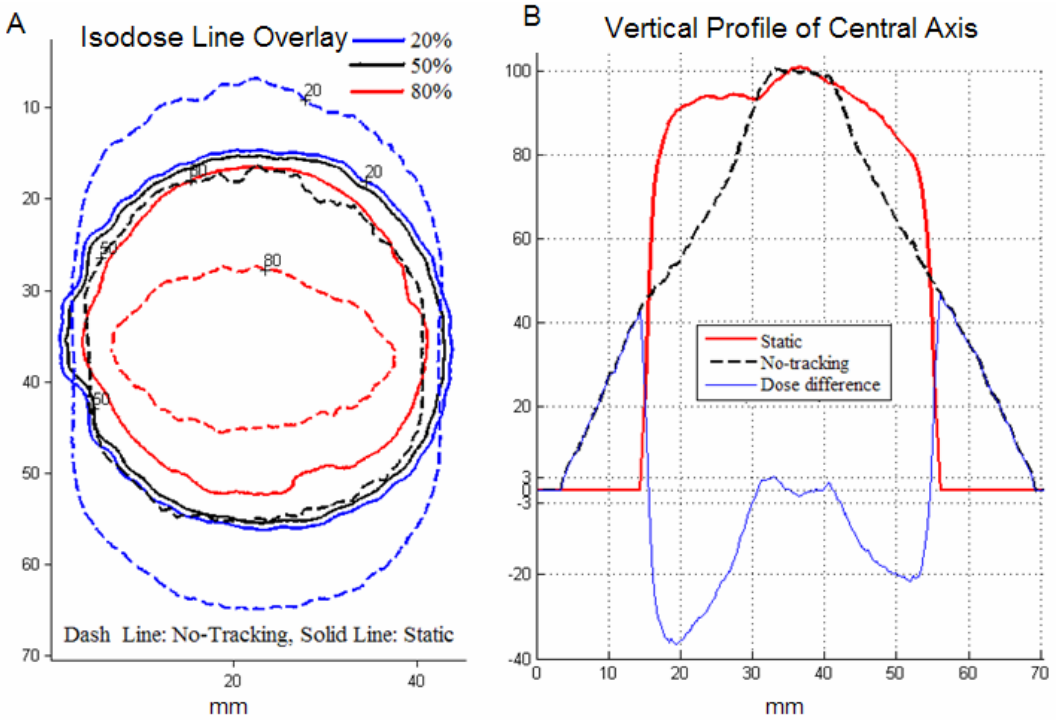

Figure 8 (A) Isodose line comparisons and (B) Vertical profile of central axis between the No-tracking (Dash line) and Static (Solid line) patterns

Neither the isodose line overlay, nor the dose profile is capable of showing the whole planar dose difference for two films. The No-tracking pattern was subtracted by the film of Static pattern after we registered and normalized the two films, as shown in Figure 9a). The dose difference is referenced by the color bar, a positive sign meaning the No-tracking pattern dose is higher than the reference Static pattern; a negative sign meaning less.

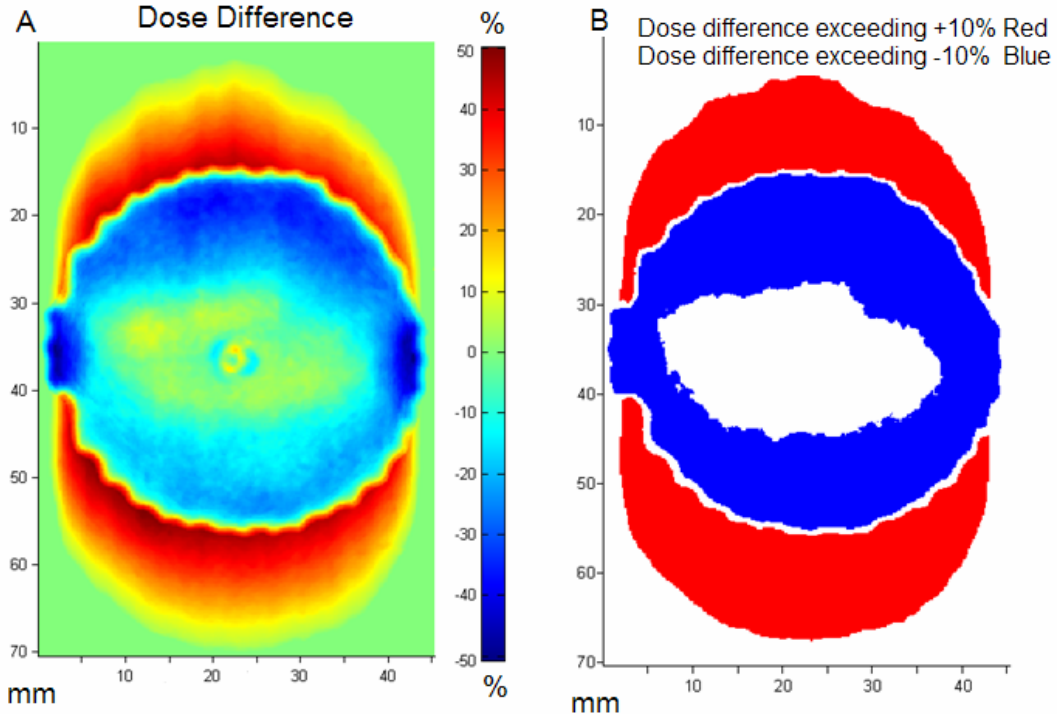

Figure 9 (A) Dose differences over the resulting irradiation field, and (B) film areas with 10% or more dose difference from subtracting dose maps of No-tracking from that of Static irradiation fields.

To further analyze the dose difference, we set up a tolerance of 10% and calculated the percentage of area in which the dose difference is over the tolerance, as shown in Figure 9b). The under-dose area (less than -10%) in high dose region was 27.05% less than static irradiation field, while the over-dose area (higher than +10%) in low dose region along SI direction was 28.5% more than static irradiation field.

3.3.2 Static pattern VS Tracking pattern

Dosimetric comparisons between static irradiation field and real-time tumor tracking situation were shown in Figure 10. From isodose distributions in Figure 10a), we can see that the introduction of real-time tumor tracking in this small, 4 cm in diameter treatment field situation, improves the tumor coverage at the 50% line removing the undulation. While the 20% dose is slightly elongated, the 80% dose is slightly reduced towards the center area.

Furthermore, Figure 10b) indicated the dose differences over the irradiation field between Static and real-time tumor Tracking patterns. In the real-time tumor Tracking pattern, the under-dose area (less than -10%) in high dose region was 5.61% less than the Static irradiation field, while the over-dose area (higher than +10%) in the low dose region along SI direction was 6.03% more than the Static irradiation field.

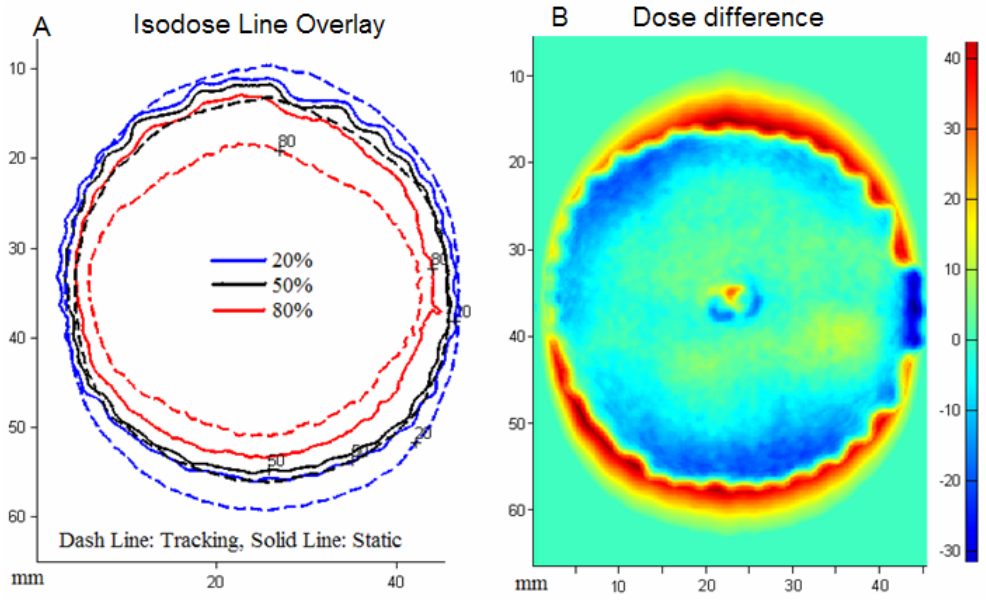

Figure 10 (A) Isodose line comparisons between real-time tumor Tracking (dashed line) and Static (solid line) situations, (B) Dose differences over the irradiation field resulting from the subtracting dose maps of real-time tumor Tracking from that of the Static irradiation field.

In our study the Static pattern is considered the ideal situation, one in which the beam conforms to a static target or one, where the moving target is perfectly tracked and thus radiated conformal. In a real patient the respiratory cycle renders such conformal radiation very difficult.

3.3.3 No-tracking pattern VS Tracking pattern

We compared with the No-tracking pattern with the Tracking pattern directly by evaluating dosimetric difference.

Figure 11 showed the isodose line overlay and the dose difference comparisons between the No-tracking situation which is commonly observed in nowadays radiation treatments and the newly introduced real-time tumor Tracking

situation that can be achieved using the DmMLC. Contrasting the real-time tumor Tracking situation, the No-tracking pattern gave smaller high dose coverage, while it resulted in extended and distorted low dose distribution. As we set a +/- 10% criteria of the expected dose to evaluate the area-proportion that exceeds our tolerance over the irradiation field, we observed that in the No-tracking pattern the high dose region is approximately 22.6% smaller. The low dose region is approximately 26.6% bigger, compared to the Tracking pattern result. This result directly indicates the improvement of the real-time tumor tracking technique for its better tumor coverage while sparing normal tissue around the tumor edge in respiratory motion direction (assumed to be only SI direction in our study) in this small treatment field situation.

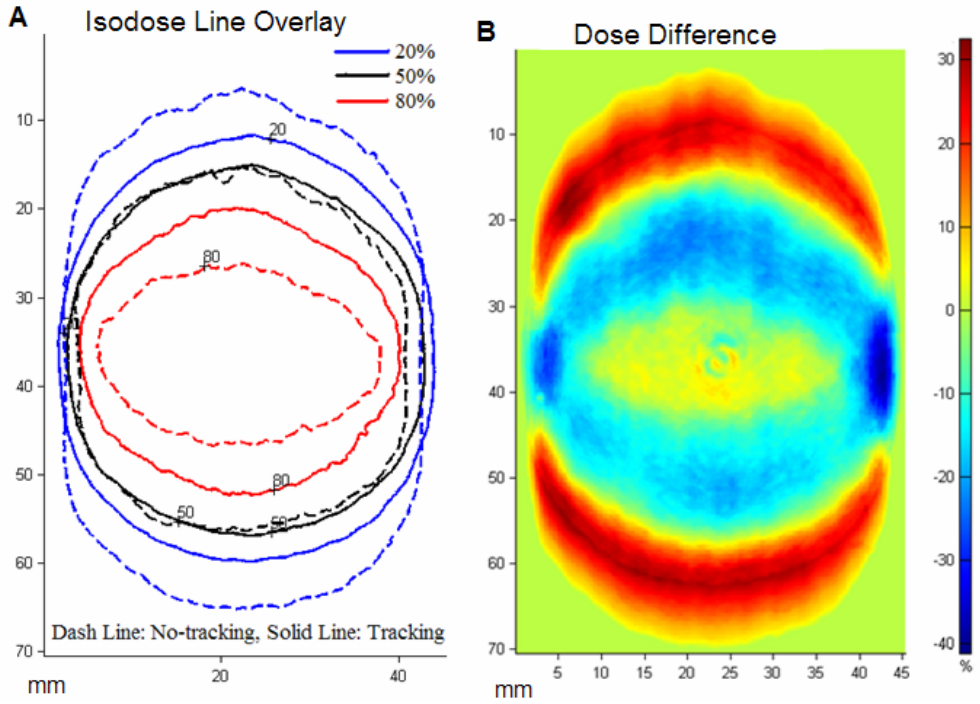

Figure 11 Isodose line comparisons between no tumor tracking (dashed line) and real-time tumor tracking (solid line) situations, (B) Dose differences over the irradiation field resulting from subtracting dose map of real-time tracking from that of no tumor tracking.

Table1 summarized the dosimetric comparisons among these three delivery patterns. The comparison index was set to represent the percentage (%) that is greater than +/- 10% dose difference between two different delivery patterns around the target. The dose difference between the No-tracking pattern and the Static pattern was 55.58% over the tolerance. The dose difference between the No-tracking pattern and the Tracking pattern was 49.14% over the tolerance. With tracking, the dose difference between the Tracking pattern and the Static pattern was 11.64% over the tolerance.

Table 1 Comparisons of area that exceeds +/-10% expected dose among the Static, No-tracking and Tracking patterns over the irradiation field

	Dose Difference		
Patterns Comparison (Target motion perpendicular to the beam direction)	< -10% expected dose area	> +10% expected dose area	Over the tolerance (10%)
No-tracking against Static	28.53%	27.05%	55.58%
Tracking against Static	6.03%	5.61%	11.64%
No-tracking against Tracking	26.58%	22.56%	49.14%

3.4 Dosimetric analysis of radiographic films of target motion in beam direction VS static film

Figure 12 (a) shows the Gafchromic film of static target and Figure 12 (b) shows the Gafchromic film of moving target with the same amount dose delivered. The only difference of the experimental setting up is that the target moves in the beam direction from -1 cm to 1cm from the SSD = 100 cm in the Figure 12 (b). The filed shape of the two films in Figure 12 turns out to be very close with each other.

(A) Static Target

(B) Target motion in the beam direction

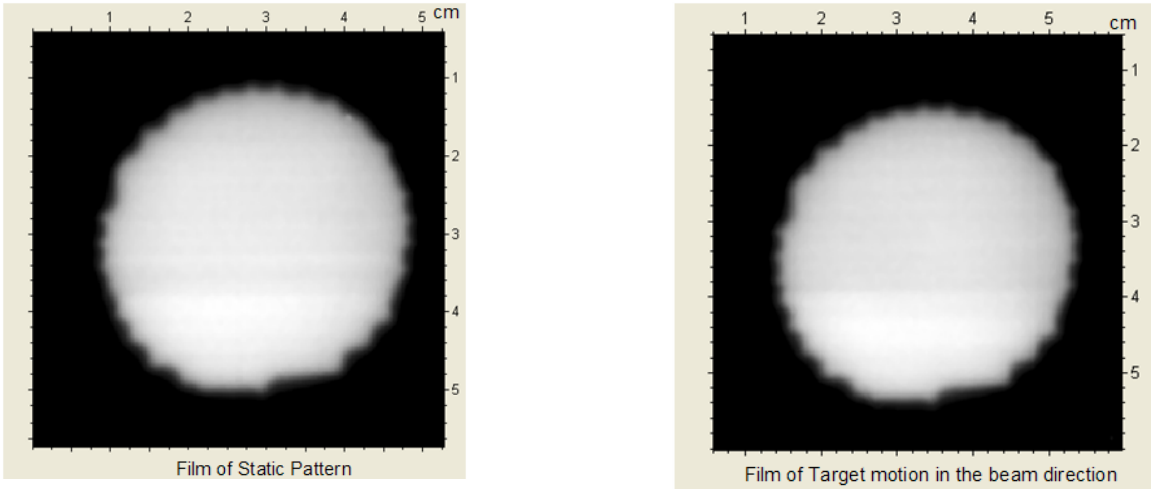

Figure 12 Radiographic films of (A) Static pattern, (B) Target motion in the beam direction

Figure 13 showed the isodose line overlay and the dose difference of the films from the static target and the moving target in the beam direction.

(A) Isodose line overlay

(B) Dose Difference

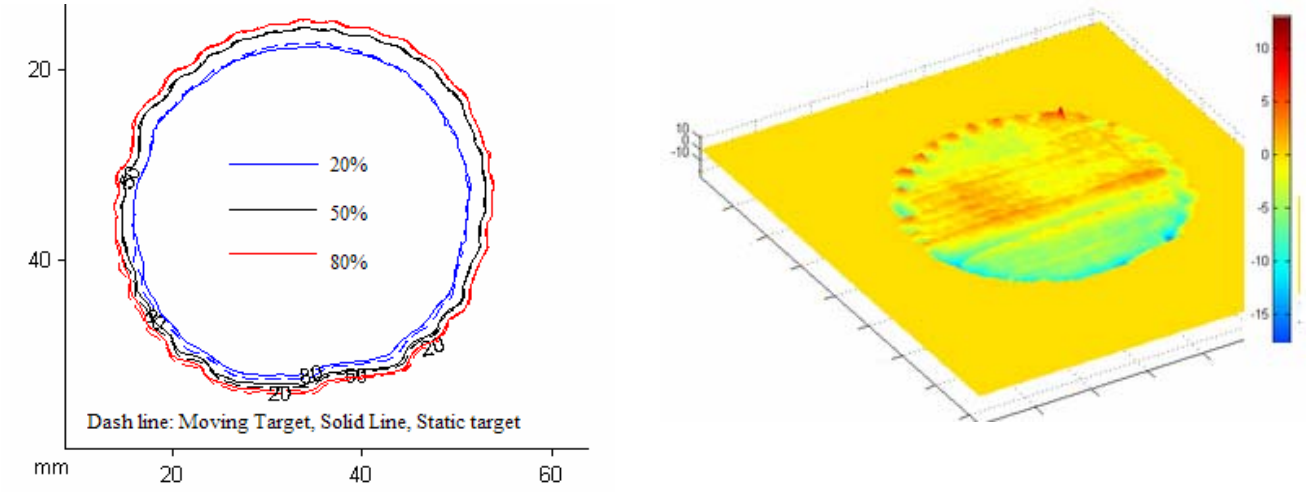

Figure 13 Isodose line comparisons and dose difference comparison, (A) Static target (solid line) and moving target (dash) situations, (B) Dose differences over the irradiation field resulting from subtracting dose map of moving target in the beam direction from that of static target.

Figure 13 (A) shows that there is only a very small difference regarding the isodose line of the films from the static target and the moving target in the beam direction. So we still use the planar dose difference to further analyze the dose difference based on pixel by pixel. Figure 13(B) shows the planar dose difference comparisons for the films of the static target and the moving target in the beam direction.

Table 2 shows the dose difference of the films from the moving target in the beam direction and the static target. The 10% tolerance in this case may not be accurate enough to show the difference, three additional tolerances (5%, 3% and 1%) were

selected. The dose difference exceeding the tolerance for the moving target and static target are 1.11%, 4.52%, 9.50% and 19.63% when the tolerance was selected as 10%, 5%, 3% and 1% respectively.

Table 2 Comparisons of area that exceeds the tolerance of the moving target in the beam direction against the static target

	Dose difference exceeding +/- tolerance			
Tolerance Selection	10%	5%	3%	1%
In beam direction moving target against Static target	1.11%	4.52%	9.50%	19.63%

For comparison of the dose difference of the moving target in the beam direction against the static target, first we selected the tolerance 10% as we used in the patterns where target moves perpendicularly to the beam direction. The dose difference exceeding the tolerance (10%) for target moving in the beam direction is 1.11%.

For the three evaluation patterns where the target moves perpendicularly to beam, the dose difference of the No-tracking against Static, No-tracking against Tracking, and Tracking against Static were 55.58%, 49.14% and 11.64% respectively. By tracking, the dose difference of the delivered dose compared to the expected dose was reduced from 55.58% (No-tracking against Static) to 11.64% (Tracking against Static), accepting tolerance below 10%. This reduction in dose difference can be considered a big improvement. The DmMLC-based tracking covers the two dimension of tumor motion, perpendicular to the beam.

The combination of Table 1 and Table 2 demonstrated that missing a target (perpendicular to the beam direction) has a much more significant effect on dose than changes in SSD (movement in the beam direction).

3.5 Tracking failure assessment

In the real-time tracking experiments, there exist three types of failure as mentioned above in which the RTRT system lost the tracking of the moving tumor.

First, we used various diameter of golden marker ranging from 1 mm to 5 mm. A 1 mm marker turned out not big enough to give the clear contrast for IPT to process. Selecting marker size bigger than 2.0 mm, lead to successful detection of marker contrast. The IPC was capable of detecting the marker and provided the right marker trajectory.

To evaluate tracking efficiency due to various marker motion speeds, the respiratory phantom cycle changed from 4 seconds to 6 seconds, and the motion elongation between the end-inhale and end-exhale positions changed from 10 mm to 40 mm. The marker speed ranges from 3.3 mm/second to 20 mm/second. At marker speeds in excess of 15 mm/second, tracking failure occurred.

The third failure scenario was unexpected systematic failure. Using the optimal marker size (2 mm in diameter) and the ideal marker speed (12 mm/second) we repeated the same experiment configuration (marker elongation 30 mm, 5 second cycle). After repeating the same tracking situation up to 70 times, we happened to have one tracking failure.

4 Discussion

4.1 Rigid/Deformed Target

With this phantom based experiment, we have successfully validated the tracking capabilities of the DmMLC. Currently, we do not change the shapes formed by the DmMLC leaves. Therefore, a clinical implementation would assume a rigid transformation of the PTV with only shift—but not rotation—taken into account. Such a rigid transformation can be applied in clinical situations where the target does not deform or deforms minimally with motion. One such example was reported

by Deurloo et al (2005) who found that the prostate exhibits shape deformations that are small relative to its motion. A first order correction, therefore is feasible for setup errors and organ motion only.

Traditionally, movement has been compensated for by greater margins, practically placing a CTV under a stationary beam at any time. Assuming further an almost uniform density of the prostate and immediate surrounding tissue, our real-time tracking system allows for the PTV placement such that CTVs move within a dose cloud. Volume-dose distributions are clearly affected by the number of treatment fields and displacement magnitude but the homogeneity of surrounding tissues has to be considered equally. Studies in the lung by Engelsman et al and Beckham et al have both found dose-errors of 5%; however, the change of equivalent uniform dose found was 0.5%. The dependency of accurate dose calculation on PTV-location and size has also been investigated by Rassiah et al (2006). Therefore with the appropriate algorithm chosen, it could be argued that for realistic organ displacements and multiple field treatments the dose-error due to density changes is small. This renders the delivered dose invariant to tissue displacement (Bortfeld, et al. 2004) as long as full coverage of the CTV is achieved.

We have tested the system with symmetric movements and one target size only. Tracking non-regular targets and application of tracking from various beam-direction, as experienced in real treatments will be done. Testing of periodic-asymmetric motion tracking, as exhibited by many organs affected by breathing (for example, liver) and further, testing of realistic motion patterns is needed to understand and account for motion-drift over prolonged periods of treatment. Evaluation of the effects of rapid changes of motion, i.e. coughs with the tracking system will be conducted in the future.

5 Conclusion

The real-time tracking delivery provides an opportunity to achieve more conformal coverage of tumor tissue and reduces the dose delivery to normal tissue at the same time. The dose difference of radiographic films between the No-tracking pattern and the Static pattern was 55.58% over the selected tolerance of 10%. The dose difference between the No-tracking pattern and the Tracking pattern was 49.14% over the tolerance. With tracking, the dose difference between the Tracking pattern and the Static pattern was 11.64% over the tolerance.

After the IMRT and IGRT, the 4D delivery and real-time tracking is the next focus in radiotherapy. The TracKnife system offers a State-of-the-art medical technique for future needs. Currently, the rigid apertures were successfully generated during the real-time tracking. Motivated by the results on this RTRT, the next challenge may lead to accommodation of deformed motion tracking.

Acknowledges

The research was financially supported by Initia-RT for providing the DmMLC and the prototype of TrackBeam.

Reference

Azuma, R. T., & Bishop, G. (1994). Improving Static and Dynamic Registration in an Optical See-Through HMD, Computer Graphics (SIGGRAPH 94 Conference Proceedings ed., pp. 197-204). Orlando, FL USA: ACM Press, Addison-Wesley.

Beckham W.A., Keall P.J., Siebers J.V., A fluence-convolution method to calculate radiation therapy dose distributions that incorporate random set-up error. Physics in Medicine and Biology, 2002. 47(19):3465-3473.

Bortfeld T, Jokivarsi K, Goitein M, et al: Effects of intra-fraction motion on IMRT dose delivery: Statistical analysis and simulation. Phys Med Biol 47:2203-2220, 2002

Bortfeld T, Jiang SB, Rietzel E. Effects of Motion on the Total Dose Distribution. Seminars in Radiation Oncology, Vol 14, No.1 (January), 2004: pp 41-51

Brandner E.D., Wu A., Chen H. et al. Abdominal Organ Motion Measured Using 4D CT. Int. J. Radiation Oncology Biol. Phys, Vol.65, No. 2, pp. 554-560, 2006

Bucciolini M, Russo S, Buonamici FB, et al. Dosimetric characterization of a Bi-directional Micromultileaf Collimator for Stereotactic applications. Med. Phys. 29 (7), July 2002

Butson, M. J., Cheung, T., and Yu, P. K., 2006. Weak energy dependence of EBT Gafchromic film dose response in the 50 kVp-10 MVp X-ray range Appl Radiat Isot 64(1) 60-2.

Cheung, T., Butson, M. J., and Yu, P. K., 2006. Independence of calibration curves for EBT Gafchromic films of the size of high-energy X-ray fields Appl Radiat Isot 64(9) 1027-30.

Devic, S., Seuntjens, J., Hegyi, G., Podgorsak, E. B., Soares, C. G., Kirov, A. S., Ali, I., Williamson, J. F., and Elizondo, A., 2004. Dosimetric properties of improved Gafchromic films for seven different digitizers Med. Phys. 31(9) 2392-401.

Deurloo, K.E.I., et al., Quantification of shape variation of prostate and seminal vesicles during external beam radiotherapy. International Journal of Radiation Oncology, Biology, Physics, 2005. 61(1):228-238.

Devic, S., Seuntjens, J., Sham, E., Podgorsak, E. B., Schmidtlein, C. R., Kirov, A. S., Soares, C. G., 2005. Precise radiochromic film dosimetry using a flat-bed document scanner Med. Phys. 32(7) 2245-53.

Dietrich L, Tuecking T, Nill S, Oelfke U. Compensation for respiratory motion by gated radiotherapy: an experimental study. Phys.Med.Biol. 50 (2005) 2405-2414

D'Souza D et al. Real-time intra-fraction-motion tracking using the treatment couch: a feasibility study. 2005 Phys. Med. Biol. 50 4021-4033

[1]Liu Y, Shi C, Lin L, Papanikolaou N. 4D dynamic intensity modulated radiation treatment with dual-layer micro multileaf collimators. Int J Radiat Oncol Biol Phys 2007; 69(3), 697

[2]Liu Y, Shi C, L Lin, Papanikolaou N. Evaluation of a dual-level micro multileaf collimator in reducing dose undulation and leakage. Med Phys 2007; 34(6), 2449

[3]Liu, Y., Shi, C., Tynan, P., Papanikolaou, N. Dual layer MLC dosimetric characteristics for small field and IMRT applications. J. Appl Clin Med Phys (Accepted, Dec 2007)

Engelsman, M., et al., The effect of breathing and set-up errors on the cumulative dose to a lung tumor. Radiotherapy and Oncology, 2001. 60(1): 95-105.

Foxlin, E., Harrington, M., & Pfeifer, G. (1998). Constellation™: A Wide-Range Wireless Motion-Tracking System for Augmented Reality and Virtual Set Applications. In M. F. Cohen (Ed.), Computer Graphics (SIGGRAPH 98 Conference Proceedings ed., pp. 371-378). Orlando, FL USA: ACM Press, Addison-Wesley.

Gamble, L. M., Farrell, T. J., Jones, G. W., and Hayward, J. E., 2003. Composite depth dose measurement for total skin electron (TSE) treatments using radiochromic film Phys. Med. Biol. 48(7) 891-8.

George R, Chung TD, Vedam SS, et al. Audio-Visual Biofeedback For Respiratory-Gated Radiotherapy: Impact of Audio Instruction and Audio-Visual Biofeedback on Respiratory-Gated Radiotherapy. Int. J. Radiation Oncology boil. Phys., vol. 65, No.3, pp. 924-933, 2006

Greg Welch, Gary Bishop, An Introduction to the Kalman Filter, SIGGRAPH 2001, Los Angeles, CA, August 12-17, 2001

Harvey, A.C. Forecasting, Structural Time Series Models and the Kalman Filter. Cambridge University Press, Cambridge, 1989.

Hugo GD, Yan D, Liang J. Population and patient-specific target margins for 4D adaptive radiotherapy to account for intra- and inter-fraction variation in lung tumor position. Phys. Med. Biol. 52 (2007) 257–274

International special products (ISP) corp., 2006. Gafchromic® EBT self-developing film for radiotherapy dosimetry user's manual.

Julier, Simon J. and Jeffery K. Uhlmann. A New Extension of the Kalman Filter to nonlinear Systems. In The Proceedings of AeroSense: The 11th International Symposium on Aerospace/Defense Sensing, Simulation and Controls, Multi Sensor Fusion, Tracking and Resource Management II, SPIE, 1997.

Kalman, R. E. A New Approach to Linear Filtering and Prediction Problems. Transactions of the ASME - Journal of Basic Engineering Vol. 82: pp. 35-45 (1960).

Kalman, R. E., Bucy R. S., New Results in Linear Filtering and Prediction Theory. Transactions of the ASME - Journal of Basic Engineering Vol. 83: pp. 95-107 (1961).

Keall PJ, Joshi S, Vedam SS, et al. Four-Dimensional Radiotherapy Planning for DMLC-based Respiratory Motion Tracking. Med. Phys. 32(4), April 2005

Kubo HD, Wang L. Compatibility of Varian 2100C gated Operations with Enhanced Dynamic Wedge and IMRT Dose Delivery. Med. Phys. 27 (8), August 2000.

Lujan A E et al 1999 A method for incorporating organ motion due to breathing into 3D dose calculations Med. Phys. 26 715–20

Mageras GS, Yorke E. Deep Inspiration Breath Hold and Respiratory Gating Strategies for Reducing Organ Motion in Radiation Treatment. Seminars in Radiation Oncology, Vol 14, No.1 (January), 2004: pp 65-75

Murphy, MJ. Tracking Moving Organs in Real Time. Seminars in Radiation Oncology, Vol.14, No.1 (January), 2004: pp 91-100

Rassiah-Szegedi, P., et al., Monte Carlo characterization of target doses in stereotactic body radiation therapy (SBRT). Acta Oncologica, 2006. 45(7): 989-994.

Schweikard A, Shiomi H, Adler J., 2004. Respiration tracking in radiosurgery. Med Phys. 31(10):2738-41.

Su F. C., Liu Y. X., Stathakis S., Shi C.Y., Esquivel C., Papanikolaou N. Dosimetry characteristics of GAFCHROMIC® EBT film responding to therapeutic electron beams. Appl Radia Iso 2007; 65: 1187-1192.

Shirato Hiroki, Yvette Seppenwoolde, Kitamura Kei et al., 2004 Intra fractional Tumor Motion: Lung and Liver. Seminars in Radiation Oncology, 114(1), 10-18

Todorovic, M., Fischer, M., Cremers, F., Thom, E., and Schmidt, R., 2006. Evaluation of Gafchromic EBT prototype B for external beam dose verification Med. Phys. 33(5) 1321-8.

Vedam SS, Keal PJ, Kini VR, Mohan R. Determining Parameters for Respiration-Gated Radiotherapy. Med. Phys. 28 (10), October 2001

Zhang T, Respiratory Gating and 4-D Tomotherapy. PhD Thesis. Med. Phys. 31 (12), December 2004